ACS OMEGA

http://pubs.acs.org/journal/acsodf
Article

Influence of Tectonically Deformed Coal-Based Activated Carbon and Its Surface Modification on Methane Adsorption

Xuan Huan, Xiaojie Guo,* Xuexi Chen, and Xin Guo

Cite This: *ACS Omega* 2024, 9, 33510−33521
Read Online

ACCESS | Metrics & More | Article Recommendations | Supporting Information

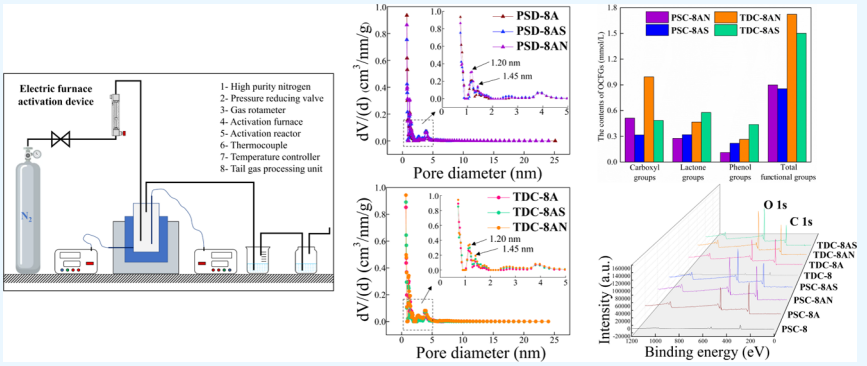

ABSTRACT: A series of coal-based activated carbons (CACs) were synthesized from mylonitized fat coal, a type of tectonically deformed coal (TDC) and symbiotic primary structural coal (PSC), followed by oxidative modification. The pore structure, surface oxygen-containing functional groups, and their influence on methane adsorption by CAC as the simplified coal model were investigated by using low-temperature nitrogen adsorption, Fourier transform infrared spectroscopy, Boehm titration, and X-ray photoelectron spectroscopy. The results showed that tectonic deformation fostered smaller pores, particularly ultramicropores in TDC, dominating methane adsorption. Acid-modified TDC-based activated carbons (ACs) showed higher pore parameters and oxygen-containing functional groups than those of PSC-based ACs. Nitric acid introduced abundant carboxyl groups concurrently increasing the pore volume and specific surface area (SSA), while sulfuric acid−ammonium persulfate treatment resulted in increased lactone groups and a partial collapse/blockage of nanopores. Methane adsorption experiments confirmed the importance of micropores and revealed a significant decrease in capacity owing to increased oxygen-containing functional groups as the primary role, with pore wall corrosion playing a secondary role. Thus, the study highlights the surface effects of TDC on methane adsorption and the potential for producing high-performance methane storage materials from China's tectonic coal resources.

1. INTRODUCTION

Coalbed gas comprising methane represents an unconventional energy resource. However, it is responsible for severe mining safety incidents, particularly coal and gas outbursts.[1−3] The efficient extraction and rational utilization of coalbed gas are vital for green transformation and the smooth realization of the dual carbon strategy of the energy sector of China,[4−6] mitigating mine gas disasters, and substantially alleviating environmental pressure.[7] An in-depth investigation of methane adsorption by coal has been the central focus of gas geology research.[8,9]

Coal comprises a heterogeneous and complex porous structure, which is important in the storage and transport of coalbed methane.[10] The adsorption, desorption, and diffusion of methane depend on the porous structure of the coal. A subtle variation of the porous structure can profoundly affect the overall distribution of methane.[8] Qiu summarized that methane is predominantly adsorbed by micropores owing to their large specific surface area (SSAs) with abundant adsorption sites.[11] Hence, the large SSA of coal governs its methane adsorption capacity. Wei and Song[12,13] emphasized that micropores and transition pores dominated gas adsorption through their combined pore volumes and surface areas at low pressure; methane was adsorbed on the walls of mesopores and macropores with increasing pressure. Li[14] revealed distinctive fractal characteristics in the pore structures of differently ranked coal samples, displaying an asymmetric U-shaped pattern and reflecting the influence of coalification on pore fractal dimensions. Jia et al.[15] revealed that the greater tortuosity of the middle- and low-ranked coal was responsible

Received: January 30, 2024
Revised: July 9, 2024
Accepted: July 11, 2024
Published: July 24, 2024

https://doi.org/10.1021/acsomega.4c00978
ACS Omega 2024, 9, 33510−33521

Table 1. Proximate and Ultimate Analysis Results of Coal Samples[a]

sample no.	deformation degree	proximate analysis (wt %)			ultimate analysis (wt %, daf)				
		M_{ad}	A_{ad}	V_{daf}	C	H	N	S	O*
PSC-8	primary structural coal	1.34	14.49	34.56	87.23	5.75	1.24	1.03	4.75
TDC-8	tectonically deformed coal	1.65	16.86	37.49	87.69	5.21	1.10	1.11	4.89

[a]M, moisture; A, ash yield; V, volatile matter; ad, air-dried basis; daf, dry ash-free basis; O, oxygen; *, by difference.

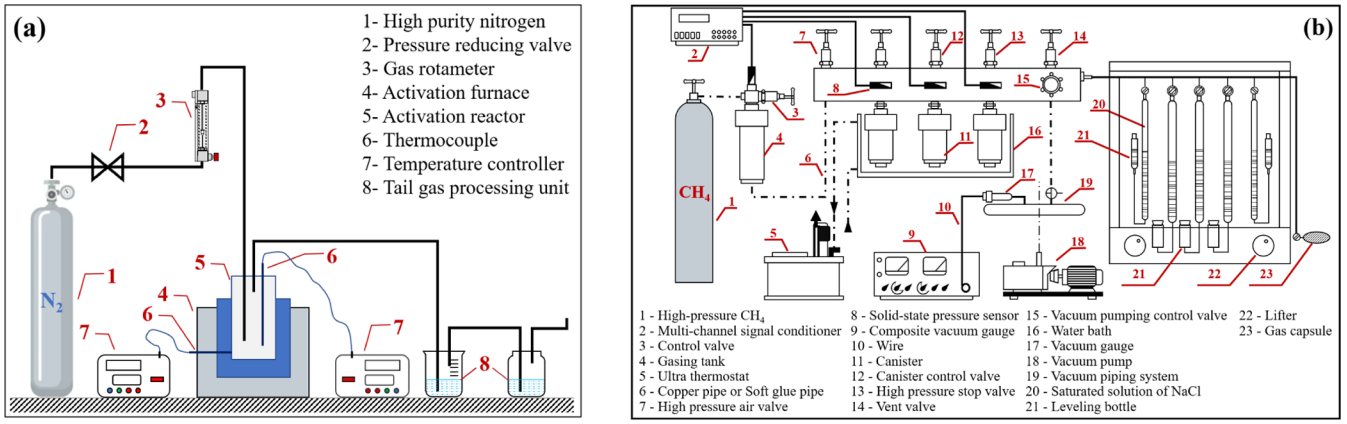

Figure 1. Schematic representation of (a) activated carbon prepared by heating using an electrical furnace and (b) a high-pressure adsorption process.

for a low methane uptake. Oxygen-containing functional groups (OFGs) on the coal surface influenced methane adsorption behavior by interacting with methane molecules.[16,17] Sun et al.[18] revealed that the gas adsorption capacity was negatively correlated with the ash content and OFGs, while positively correlated with the vitrinite content in a study via synchrotron radiation nanocomputed tomography and small-angle X-ray scattering. Thus, the intricate internal structure of coal hinders the quantitative elucidation of the impact of physicochemical structures on methane adsorption behavior via direct methodologies compared to conventional solid adsorbents.[19,20]

Coal exhibits exceptional sensitivity to stress and strain.[21] The Paleozoic coal-bearing basins in China have been tectonically modified owing to extrusion, shearing, and extensional stress since the Mesozoic era, resulting in the formation of tectonically deformed coal (TDC) within the coal-bearing strata.[22−24] TDC characterized by severely damaged physicochemical structures, high adsorption, and low strength and permeability are critical preconditions for coal and gas outbursts.[25,26] The stress−strain system proposed by Ju et al.[27,28] has been adopted from the several proposed classification schemes of TDC.[29] The stress−strain system categorizes TDC into three major classes (brittle, shear/transition, and ductile TDC) and 10 subtypes. Brittle coal (cataclastic and granulitic coal) is a repository for abundant coalbed methane, whereas mylonitic coal is abundant in areas of coal and gas outburst. The abnormal behavior of TDCs is attributed to the complex pore-fracture structure, heterogeneous coal matrix, and intricate changes in mechanical properties compared to the symbiotic undeformed primary structural coal (PSC) retaining their original structure.[29] These factors influence gas occurrence, transportation properties, and the challenge of studying methane adsorption by TDC.[30,31]

Coal-based activated carbon (CAC) possesses microstructures and OFGs on the surface analogous to those of coal.[32,33] However, the surface areas and nanopore contents of CAC are higher than those of coal. The physicochemical surface properties of CAC can be tailored through appropriate acid−base modifications.[34] CAC can be used as a prevalent simplified model for investigating methane adsorption by coal[20,35] and the influencing factors based on the similar functional groups and surface characteristics of coal and CAC. However, prevailing studies rely on commercial CAC, which conventionally does not have similar parameters describing the characteristics and quality of the original coal. In addition, commercial CAC exhibits marked disparities from specific coal varieties, owing to its standardized manufacturing process, and is not suitable for exploring the impact of TDC on methane adsorption.

This study aims to address these issues by using TDC and symbiotic PSC as raw materials to synthesize and modify CACs via mild methods. The modified CAC samples were used as simplified models to overcome current limitations and investigate methane adsorption by TDC. We selected mylonitic coal with a prominent fragmented structure, ultrahigh porosity, and abundant surface active sites, owing to its severe tectonic deformation, as an ideal candidate for investigating methane adsorption properties by TDC. TDC was used as a novel feedstock for CAC synthesis for the first time, broadening the scope of feasible raw materials. The advantages of TDC over conventional coal sources based on CAC performance were explored, revealing the potential of the abundant resource. The objectives of the work are as mentioned: (i) investigating the methane adsorption mechanisms of TDC and (ii) exploring the range of raw materials to prepare CAC while revealing the distinctive attributes and substantial potential of TDC in the production of AC.

2. MATERIALS AND METHODS

2.1. Coal Samples and Basic Parameter Determination. The Pingdingshan mining area in Henan Province has been subjected to successive tectonic influence from the North China plate, Qinling-Dabie orogenic belt, and Pacific Kula

https://doi.org/10.1021/acsomega.4c00978
ACS Omega 2024, 9, 33510−33521

plate subducting in the north−northwest direction. These activities caused severe geological structural damage to form different types of TDC.[21] Our group has extensively investigated the microstructure and adsorption properties of TDC in these areas.[36−39] We selected fat coal from the Wu_{9-10} coal seam of the No. 8 mine in Pingdingshan for this study. Detailed information on the tectonic disposition of the Pingdingshan coalfield is reported earlier.[40]

The PSC-8 sample appears bright with a clear coal petrological composition and bedding. It possesses high mechanical strength and well-developed joints and lacks visible wrinkles or a structural sliding surface. Conversely, the TDC-8 sample is completely destructed from its original structure. Its petrological components, bedding, and cleavage patterns are not discernible. The coal matrix disintegrates into fine powder particles, characteristic of mylonitic coal.[27] We performed proximate and ultimate analyses of coal samples following the Chinese national standards GB/T 212-2008 and GB/T 31391-2015, and the results are presented in Table 1.

2.2. Preparation of Coal-Based Activated Carbon. A three-step hydrochloric acid−hydrofluoric acid−hydrochloric acid (HCl−HF−HCl) demineralization protocol was performed to eliminate the influence of minerals on structural quantitative analysis and subsequent activation. Analytical grade HCl and HF (procured from Shanghai Aladdin Biochemical Technology Co., Ltd., China) were used to treat 200-mesh powdered coal samples at a constant temperature of 60 °C. Specific procedures were followed from the literature.[41]

CAC samples were synthesized from PSC-8 and TDC-8 via a potassium hydroxide (KOH) chemical activation method[42] using a specific activation apparatus, as illustrated in Figure 1a. TDC-8 was blended with analytical grade KOH (procured from Sinopharm) in a mass ratio of 1:1. Deionized water was added to the mixture, and the mixture was stirred to form a homogeneous mixture, which was allowed to stand for 12 h. The mixture was transferred to a nickel reactor equipped with a YFFG 150 × 400 activation furnace. The temperature was ramped up to 800 °C at 5 °C min^{-1} and maintained at 800 °C for 1 h. The mixture was allowed to cool naturally. The product was thoroughly rinsed with hot deionized water, filtered to remove unreacted KOH, and dried in a vacuum oven at 110 °C for 24 h to form TDC-based AC (TDC-8A). PSC-based AC (PSC-8A) was also prepared by following the same procedure.

2.3. Oxidative Modification of CACs. Common oxidizing agents for surface modification are nitric acid (HNO_3), phosphoric acid, hydrogen peroxide, sulfuric acid (H_2SO_4), and ammonium persulfate (APS).[43,44] Recognizing that strong oxidation can significantly increase the abundance of OFGs,[45] we selected HNO_3 and the strongly oxidative H_2SO_4−APS system. Notably, HNO_3 exhibits a sluggish reaction rate at room temperature (28 °C), primarily affecting mesoporous structures with a minimal impact on micropores. Hence, boiling conditions are imperative to ensure effective modification,[46] while care must be taken to avoid prolonged reaction time that could lead to unnecessary pore damage. Conversely, the H_2SO_4−APS system, when brought into contact with AC at 28 °C, releases substantial heat; theoretically, there is a possibility of altering the pore structure.

To ensure the investigation of pore structure variations while effectively enriching OFGs, we meticulously developed two targeted strategies: preserving the pore integrity of HNO_3-modified products and leveraging the strong corrosive nature of H_2SO_4−APS for precise control of the modified pore architectures. Here is the experimental procedure, exemplified by TDC-8A.

(1) HNO_3 modification: 300 g of TDC-8A was added to a 500 mL HNO_3 (2 mol L^{-1}) solution and was gently boiled for 3.5 h using a water bath.
(2) Combined modification of H_2SO_4−APS: 300 g of TDC-8A was added to a 500 mL saturated APS solution prepared with 1 mol L^{-1} H_2SO_4, and the reaction proceeded for 24 h at 28 °C.

The reaction mixture was filtered under vacuum after the completion of the reaction to obtain a filter cake, which was washed with deionized water until a neutral pH was obtained. The products (TDC-8AN and TDC-8AS) were vacuum-dried at 60 °C for 12 h. Identical procedures were used for PSC-8A modification, generating the CAC series presented in Table 2. HNO_3, H_2SO_4, and APS were of analytical grade and were procured from Shanghai Aladdin Biochemical Technology Co., Ltd., China.

Table 2. CAC Series and Sample Numbers[a]

sample series	CACs	HNO_3 modified CACs	H_2SO_4−APS-modified CACs
series of primary structural coal-based activated carbon	PSC-8A	PSC-8AN	PSC-8AS
series of tectonically deformed coal-based activated carbon	TDC-8A	TDC-8AN	TDC-8AS

[a]A, N, and S represent the first letters of activated carbon, nitric acid, and sulfuric acid, respectively.

2.4. Characterization of Pore Structure. Low-temperature nitrogen adsorption (LTNA) isotherms were employed to obtain detailed pore information in the range of 0.5−200 nm.[47] The SSA, pore volume, and pore size distribution of coal and CAC samples were determined using a 3H-2000 PM2 SSA and pore size analyzer.[48] In total, 2−3 g of each sample was degassed at 110 °C for 20 h to remove moisture and gaseous impurities before analysis. Nitrogen adsorption isotherms were recorded at liquid nitrogen temperature (77.35 K at 101.3 kPa) over a range of relative pressures, P/P_0 (the ratio of gas pressure to saturated vapor pressure) extending from 0.06 to 0.994. Pore structure parameters were automatically computed using specialized software, employing methodologies grounded in Brunauer−Emmett−Teller (BET), Barrett−Joyner−Halenda (BJH), and Dubinin−Radushkevich (D−R) theories for determining SSA, calculating pore volume using BJH and D−R methods, and obtaining pore size distribution (PSD) using Dubin−Astakov (D−A) model and density functional theory (DFT). An extensive explanation of these underlying theories and techniques can be found in the publications.[49−51]

2.5. Characterization of Microstructure. Before characterization, the samples were ground to below 200 mesh.

2.5.1. Fourier Transform Infrared Spectroscopy (FTIR) Analysis. FTIR was used to analyze surface functional groups on the coal and CAC samples. Experiments were conducted using the KBr pellet method using a Thermo Scientific Nicolet 380 IR spectrometer.[52,53] Each sample was scanned 32 times at ambient temperature over a range of 450−4000 cm^{-1} with a resolution of 4 cm^{-1}.

2.5.2. Boehm Titration of CACs. Boehm titration was used to quantify OFGs on the AC surface.[54] The OFGs were

https://doi.org/10.1021/acsomega.4c00978
ACS Omega 2024, 9, 33510−33521

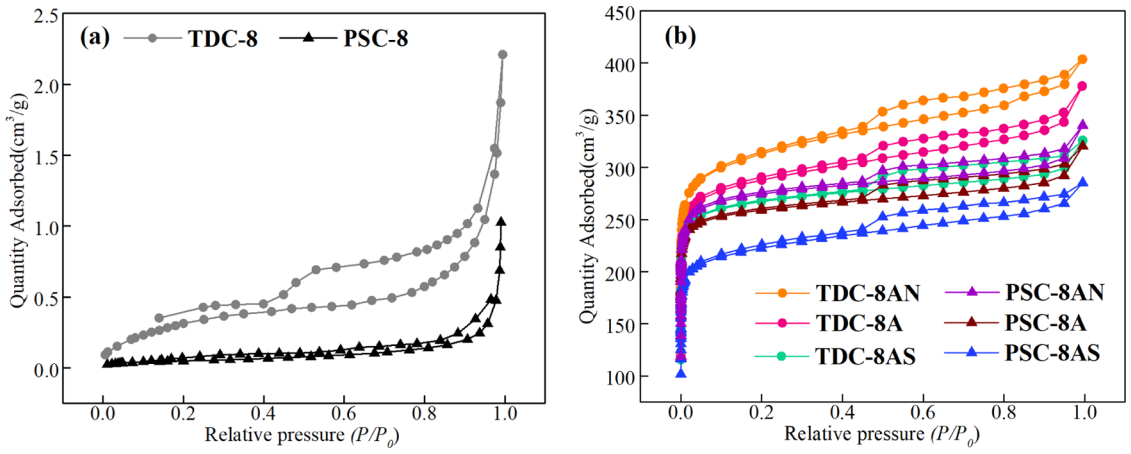

Figure 2. LTNA isotherms of coal samples (a) and the CAC series (b) at 77 K.

Table 3. Nanopore Structural Parameters of Coal Samples[a]

	pore volume/(cm^3 g^{-1})					pore volume ratio (%)			
sample no.	V_1	V_2	V_3	V_4	V_t	V_1/V_t	V_2/V_t	V_3/V_t	V_4/V_t
PSC-8	0.000705	0.000083	0.000022	0.000025	0.000835	84.43	9.94	2.64	2.99
TDC-8	0.001345	0.000433	0.000062	0.000133	0.001973	68.17	21.95	3.14	6.74
percentage added	90.78%	421.67%	181.82%	432.0%	136.29%				
	the SSA/(m^2 g^{-1})					the SSA ratio (%)			
sample no.	S_1	S_2	S_3	S_4	S_t	S_1/S_t	S_2/S_t	S_3/S_t	S_4/S_t
PSC-8	0.08043	0.02820	0.01074	0.04982	0.16919	47.54	16.67	6.35	29.45
TDC-8	0.14971	0.18685	0.07978	0.26785	0.68419	21.88	27.31	11.66	39.15
percentage added	86.14%	562.59%	642.83%	437.64%	304.39%				

[a] V_1, V_2, V_3, V_4, and V_t are the volumes of the transitional pore, micropore, mild micropore, ultramicropore, and nanopore, respectively. $V_t = V_1 + V_2 + V_3 + V_4$; S_1, S_2, S_3, S_4, and S_t are the specific surface areas of the transitional pore, micropore, mild micropore, ultramicropore, and nanopore; $S_t = S_1 + S_2 + S_3 + S_4$.

allowed to react with specific bases, followed by back-titration with a standard HCl solution to determine the amount of the neutralized base.[55] CAC samples (1 g) were added to separate 250 mL conical flasks containing 50 mL of 0.1 mol L^{-1} NaOH, Na_2CO_3, or $NaHCO_3$ solutions. The samples were shaken at room temperature for 24 h and allowed to settle overnight. The supernatant (5 mL) was titrated with a 0.05 mol L^{-1} HCl standard solution using methyl orange as an indicator. The various OFGs were neutralized following reported procedures:[56,57] $NaHCO_3$ was used for carboxyl groups, Na_2CO_3 for carboxyl and lactones, and NaOH for carboxyl, lactones, and phenolic functional groups.

2.5.3. X-ray Photoelectron Spectroscopy (XPS) Analysis. XPS was used to investigate the surface oxidation state of coal and CAC samples. Spectra were acquired using a PHI-5300/ESCA spectrometer and Al Kα radiation with a 250 W X-ray source. The analysis chamber maintained a background pressure <10^{-9} Pa. Binding energies were calibrated using the C 1s peak at 284.6 eV.

2.6. Methane Isothermal Adsorption. The impact of the altered pore and surface chemical structure in coal and CAC samples before and after modification on methane adsorption was evaluated. High-pressure adsorption experiments (Figure 1b) were conducted at 30 °C and a maximum equilibrium pressure of 5.35 MPa. Methane purity was 99.99%. The experimental protocol comprised the following steps: (i) manually separating the mineral-rich gangue from the raw coal samples to mitigate the impact of minerals on methane adsorption, and then crushing the coal samples to 60−80 mesh; (ii) weighing approximately 30 g of each sample (either raw coals or CACs), and drying them in a vacuum oven at 105 °C for 2 h to eradicate moisture; (iii) allowing the cooled samples to reach room temperature before subjecting them to vacuum at 70 °C for 8 h at a pressure <4 Pa; and, last, (iv) determining the adsorbed quantities utilizing the capacity measurement method specified in MT/T752-1997.

3. RESULTS AND DISCUSSION

3.1. Pore Structure Characteristics. The pore size of porous solids can be divided into macropores (>50 nm), mesopores (2−50 nm) and micropores (<2 nm)[58] based on the International Union of Pure and Applied Chemistry (IUPAC). However, Ju et al. proposed a natural classification method different from the IUPAC classification based on the characteristics of coal,[59] which was based on the law of mutation points in pore size distribution. The TDC nanopores (adsorption pores <100 nm) are classified into transition pores (15−100 nm), micropores (5−15 nm), mild micropores (2.5−5 nm), and ultramicropores (<2.5 nm). Given that coal is a stress-sensitive special organic rock,[21] as well as the special nanoporous and macromolecular structures of TDC, using the classification of Ju and IUPAC to characterize the nanoporous structures of coal and CAC separately is more in line with the actual situation. The LTNA isotherms of the coal and CAC samples are presented in Figure 2. Tables 3 and 4 present their respective parameters for nanopore structures.

https://doi.org/10.1021/acsomega.4c00978
ACS Omega 2024, 9, 33510−33521

Table 4. Nanopore Structural Parameters of CAC Samples[a]

sample no.	S_{BET} ($m^2\ g^{-1}$)	V_t ($cm^3\ g^{-1}$)	V_{mic} ($cm^3\ g^{-1}$)	V_{mes} ($cm^3\ g^{-1}$)	V_{mes}/V_t (%)
PSC-8A	812	0.511	0.378	0.133	26.03
PSC-8AN	863	0.533	0.391	0.142	26.64
PSC-8AS	710	0.454	0.301	0.153	33.70
TDC-8A	912	0.611	0.400	0.211	34.53
TDC-8AN	1002	0.643	0.416	0.227	35.30
TDC-8AS	839	0.520	0.388	0.132	25.38

[a] S_{BET} is the BET SSA; V_t is the total pore volume; V_{mic} is the micropore volume; V_{mes} is the mesopore volume.

Figure 2a shows the LTNA curves of coal samples. According to the IUPAC classification,[60−62] the adsorption curves increase slowly when the relative pressure $P/P_0 < 0.8$, indicating a type II adsorption isotherm. The transition from monolayer adsorption to multilayer adsorption by coal samples possessing a continuous and complete pore system is indicated. The adsorption amount by TDC-8 is higher than that by PSC-8, suggesting the superior development of macropores and transitional pores in TDC. Both samples show a sharp increase in the adsorption quantity without saturating as the pressure approaches saturation, indicating that capillary condensation and multilayer adsorption occur simultaneously.

TDC-8 displays a strikingly evident hysteresis loop ($P/P_0 > 0.5$) than that of PSC-8,[63] which indicates higher pore connectivity and the presence of more open and semiclosed pores. The hysteresis loop of TDC-8 exhibits a sharper variation at P/P_0 of 0.5 compared to that of PSC-8. This distinction further reveals that TDC-8 comprises excess bottle-shaped and slit-shaped pores with a closed end,[29] whereas PSC-8 comprises cylindrical pores with two open ends and slit-shaped pores with all open sides, and a few bottle-shaped pores.

Table 3 indicates that transitional pores dominate PSC-8. Nanopores increase during the transition from PSC-8 to TDC-8. The volume and SSA of transitional pores, micropores, mild micropores, and ultramicropores of TDC-8 increase by 90.78 and 86.14, 421.67 and 562.59, 181.82 and 642.83, and 432.0 and 437.64%, respectively. Thus, tectonic deformation facilitates the development of various nanopores. The volume and SSA ratio of transitional pores of TDC-8 decrease compared to those of PSC-8. Alternately, the volume and SSA ratio of micropores, mild micropores, and ultramicropores of TDC-8 increase more than those of PSC-8. The transitional pores during the formation process of TDC are surpassed by micropores, mild micropores, and ultramicropores, as indicated by the changes in the volume ratio and SSA ratio. Tectonic deformation contributes to the formation of pores with small diameters.[64] The SSA of ultramicropores in TDC-8 dominates, providing more adsorption sites for methane.[65,11]

Prior to delving into Figure 2b and Table 4, a pivotal aspect of our methodology merits emphasis. Conventionally, the ratio of carbon to KOH in the synthesis of CAC ranges from 1:1 to 1:5. A high ratio of 1:5 achieves an ultrahigh SSA of 4012 $m^2\ g^{-1}$, total pore volume of 2.07 $cm^3\ g^{-1}$, and average pore size of 3.56 nm.[66] However, it might obscure the distinction among CAC samples derived from different coal sources. Our strategy

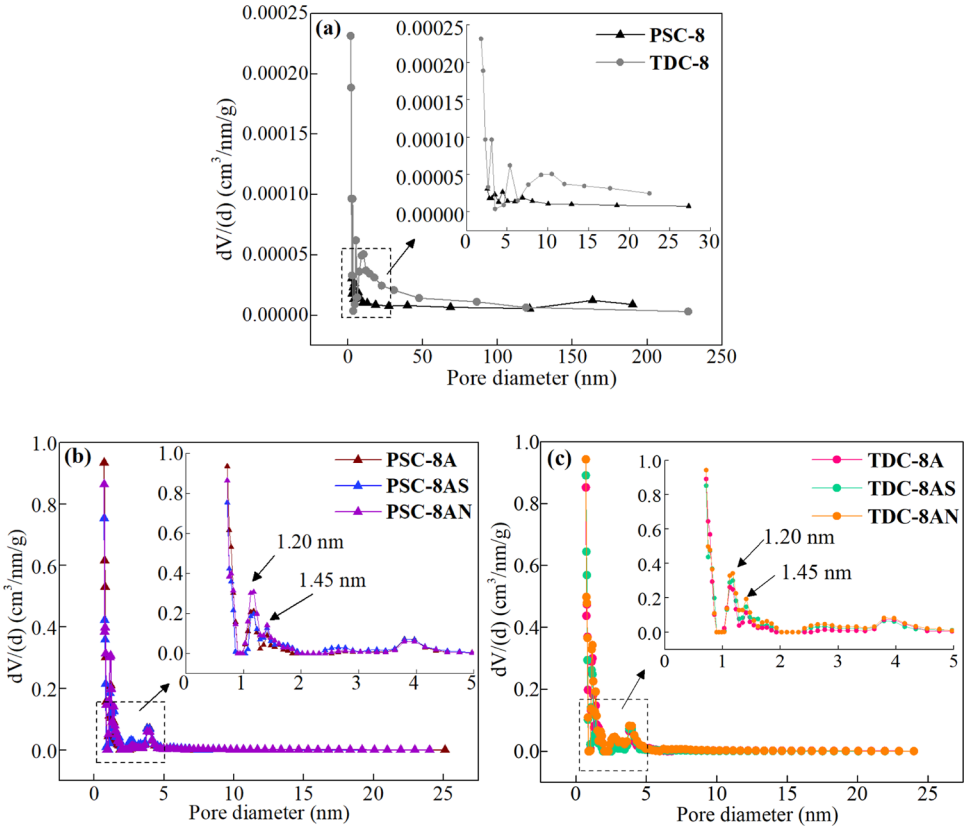

Figure 3. Pore size distribution of the samples. (a) Comparison in coals: PSC-8 versus TDC-8. (b, c) Comparison in both PSC- and TDC-based AC series. Insets represent magnified views of the 0−5 nm pore size range for detailed examination.

https://doi.org/10.1021/acsomega.4c00978
ACS Omega 2024, 9, 33510−33521

focuses on enhancing the key properties of the precursors without eradicating their individuality. Consequently, we opted for a minimal ratio of 1:1 to preserve the distinctive porosity structures and innate functional groups of each CAC, thus preventing the homogenization of the final products.

Figure 2b shows that the nitrogen adsorption capacity of CAC samples increases by 200- to 300-fold, and the adsorption curve is similar to Type I of the IUPAC standard dominated by filling of micropores ($P/P_0 < 0.1$) and monolayer adsorption.[62] The adsorption by micropores with diameters of <2 nm increases rapidly. The adsorption/desorption hysteresis loops of P/P_0 in the range of 0.4−1 show that an increase in the relative pressure induces monolayer and multilayer adsorption by mesopores, which agglomerate at the saturated pressure, appropriately accelerating the adsorption capacity. The adsorption capacity of the TDC-based AC series is higher than that of the PSC-based AC series, indicating that the basic characteristics of a high micropore content and SSA of TDC are inherited. Furthermore, the four parameters of CACs (S_{BET}, V_t, V_{mic}, and V_{mes}) from the same coal source (Table 4) increase after HNO_3 modification but decrease after H_2SO_4−APS modification. Two exceptions should be noted: (i) the adsorption capacity of TDC-8AS is slightly lower than that of PSC-8AN and (ii) the V_{mes} of PSC-8AS is higher than that of PSC-8A, indicating that H_2SO_4−APS modification might either collapse the micropores or form mesopores, inhibiting further adsorption.

Figure 3 illustrates the PSDs of the coal and CAC samples. Figure 3a underscores TDC-8's superior nanopore abundance versus PSC-8, notably in ultramicropores (<2.5 nm) and micropores (5−15 nm), with TDC-8 presenting heightened enrichment. TDC-8 also excels in transition pores (15−100 nm). Figure 3b,c illustrates a common trend: the nanopores of CACs cluster densely below 5 nm, peaking near 1.2 nm and secondarily at 1.45 nm, with negligible variation beyond this range. Zooming into the 0−5 nm interval to assess acid modification effects, HNO_3 (PSC-8AN, TDC-8AN) notably bolsters peak intensities at both key widths, whereas H_2SO_4−APS treatment elevates PSC-8AS's 1.45 nm peak but diminishes the peak at 1.2 nm for both samples. Regarding mesopores (>2 nm), HNO_3-modified CACs see maintained or slightly enhanced distributions relative to unmodified forms, conversely, TDC-8AS post H_2SO_4−APS modification shows a reduction in pores with a size of 2−5 nm compared to TDC-8A.

Thus, the two modification methods show different results. HNO_3 increases the number of micro- and mesopores, particularly enriching micropores, thereby enhancing the adsorption capacity. Despite using a slightly boiling water bath, the concentration of HNO_3 is low and the reaction time is short, which expands and loosens the original pore system of CAC. Although combined H_2SO_4−APS modification is performed at room temperature, the concentration of the mixed solution is high, and the reaction time is long. A substantial amount of heat is released in contact with PSC-8A and TDC-8A, inducing intense oxidative reactions that result in corrosion of the surface and pore walls. Thus, a few nanopores in TDC-8AS and PSC-8AS are collapsed or blocked. Specifically, PSC-8AS is predominantly affected in micropores below 1.2 nm, whereas TDC-8AS, owing to its inheritance of weak structural characteristics and high porosity from TDC,[21] experiences a comprehensive collapse or blockage, affecting both micropores and mesopores alike (Figure 3b,c). This, in turn, leads to substantial reductions in their respective pore volumes and SSAs.

3.2. Molecular Structure Characteristics. *3.2.1. FTIR Spectra of Coal and CAC Samples.* The baseline corrected FTIR spectra of the demineralized coal samples and the synthesized CAC series are shown in Figure 4. Coal and CAC

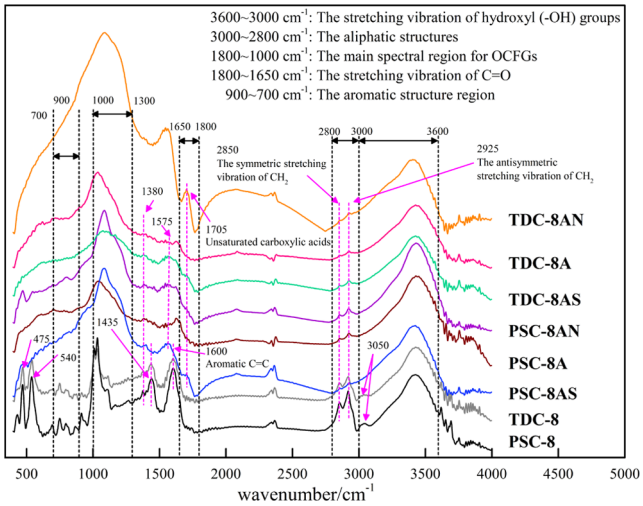

Figure 4. FTIR spectra of coal samples and the CAC series.

samples have similar microstructures, and the positions of FTIR spectral characteristic peaks are similar, but the intensity varies considerably. The peaks are assigned based on reported values[67,68] with a particular emphasis on the changes in OFGs.

The strong and broad absorption peak at 3600−3000 cm^{-1} corresponds to the stretching vibration of hydroxyl (−OH) groups. Hydroxyl groups are the main acidic OFGs in coal and CAC samples capable of binding with different acceptors via hydrogen bonds.[69] Painter et al.[70] indicated six types of hydroxyl groups: free (~3620 cm^{-1}), aromatic ring bonded (Ar−OH or OH−π; ~3500 cm^{-1}), self-associated (~3410 cm^{-1}), ether oxygen bonded (OH−ether; ~3300 cm^{-1}), cyclic associative hydrogen bonds (OH−cyclic; ~3200 cm^{-1}), and nitrogen bonded (OH−N; ~3050 cm^{-1}) hydroxyl groups. The intensity of the characteristic peaks of TDC-8 is slightly less than that of PSC-8, indicating that tectonic deformation causes oxygen loss in coal. The hydroxyl content increases, enhancing the surface polarity of CACs.[71]

The absorption bands in the range of 3000−2800 cm^{-1} are assigned to aliphatic structures. The two characteristic peaks at 2850 and 2925 cm^{-1} correspond to CH_2 symmetrical and antisymmetrical stretching vibrations, respectively.[72] Figure 4 shows that the concentration of aliphatic hydrocarbons in the CAC series is lower than that of coal samples, indicating that the aliphatic groups on the coal surface rapidly oxidize and decompose during the formation of AC.

The 1800−1000 cm^{-1} region indicates OFGs, excluding hydroxyl groups.[69] The deformation vibrations of CH_2 and CH_3 appear at 1435 and 1380 cm^{-1}, and the stretching vibration of aromatic C=C appears at 1600 cm^{-1}. The band at 1800−1650 cm^{-1} corresponds to the stretching vibration of C=O attributed to carbonyl (−C=O) and carboxyl (−COOH) groups.[73] Figure 4 shows that the absorption band of acid-modified CACs is enhanced. A well-defined peak at 1705 cm^{-1} in the modified CAC series is attributed to unsaturated carboxylic acids, indicating an increase in the

https://doi.org/10.1021/acsomega.4c00978
ACS Omega 2024, 9, 33510−33521

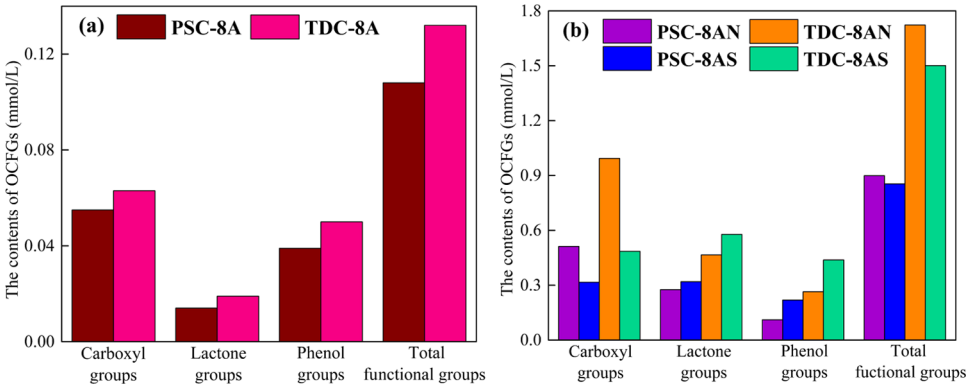

Figure 5. Oxygen-containing functional groups on the CACs surface (mmol g^{-1}): (a) unmodified CAC samples and (b) modified CAC samples.

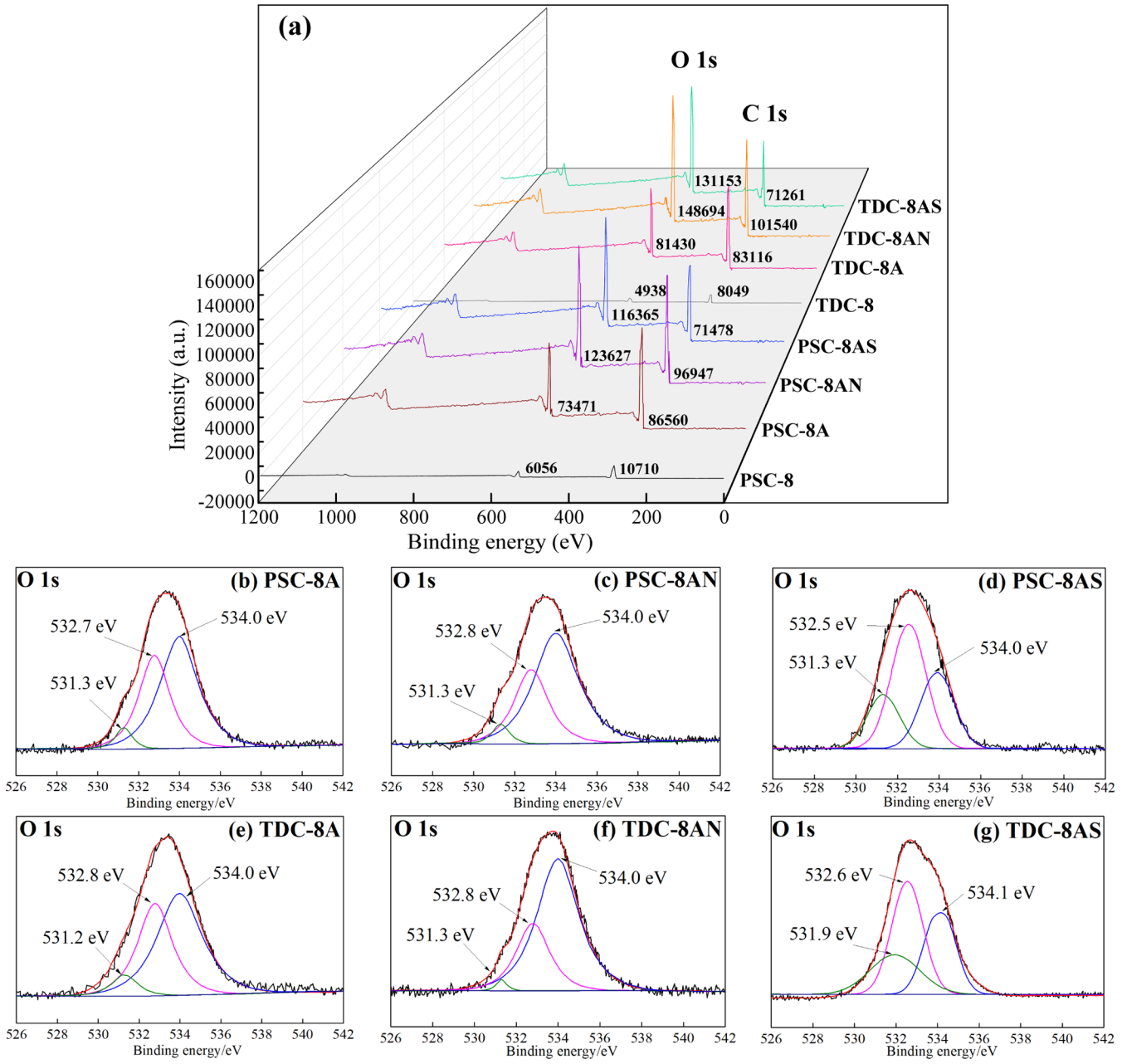

Figure 6. XPS spectrum: (a) survey scans comparing coal samples and the CAC series; (b–d) high-resolution O 1s spectra for PSC-8A, PSC-8AN, and PSC-8AS; (e–g) high-resolution O 1s spectra for TDC-8A, TDC-8AN, and TDC-8AS.

https://doi.org/10.1021/acsomega.4c00978
ACS Omega 2024, 9, 33510−33521

number of carboxylic acid groups on the surface of the acid-oxidized CACs. The absorption peak at 1575 cm^{-1} corresponds to lactones. The bands in the range of 1300−1000 cm^{-1} correspond to lactone, ether bonds, and a few oxygen−heterocyclic bonds.[74] The peak areas of the samples increase in the order of coal samples < CACs < modified CACs. Thus, OFGs, particularly carboxyl groups, and lactones, increase on the acid-treated CACs surface.

Table 1 indicates that coal samples comprise a few impure atoms, such as organic sulfur and nitrogen, which potentially influence the subsequent methane adsorption process. However, Figure 4 shows that the characteristic peaks of −SH (475 cm^{-1}), −S−S− (540 cm^{-1}), and OH−N (3050 cm^{-1}) of PSD-8 and TDC-8 disappear after activation, indicating the effective removal of these impure atoms. The low contents of N and S in coal samples and their depletion during the activation process have negligible impacts on methane adsorption. Alternately, the effect of the porosity and OFGs on methane adsorption is notable. Consequently, our discussions primarily focus on the effects of porosity and OFGs on methane adsorption performance.

3.2.2. Boehm Titration of CACs. The Boehm titration method was used to quantitatively assess the alterations in functional groups of the acid-modified CAC. The resulting data presented in Figure 5 graphically illustrate the comparative contents of carboxylic, lactone, phenol, and total OFGs on the surface of CAC. The values are presented in Table S1.

Figure 5a shows that the surface of TDC-8A exhibits higher concentrations of carboxyl (0.063 mmol g^{-1}), lactone (0.019 mmol g^{-1}), phenolic (0.050 mmol g^{-1}), and total OFGs (0.132 mmol g^{-1}) than those of PSC-8A of carboxyl (0.055 mmol g^{-1}), lactone (0.014 mmol g^{-1}), phenolic (0.039 mmol g^{-1}), and total OFGs (0.108 mmol g^{-1}). The abundance of OFGs increases notably in modified CACs (Figure 5b). However, the growth rate and extent of augmentation are more pronounced for TDC-8AN and TDC-8AS than those of PSC-8AN and PSC-8AS. The total OFG content of PSC-8AN (0.899 mmol g^{-1}) and PSC-8AS (0.854 mmol g^{-1}) increases by 8.32- and 7.91-fold, respectively, whereas the same of TDC-8AN (1.723 mmol g^{-1}) and TDC-8AS (1.501 mmol g^{-1}) show higher increases by 13.05- and 11.37-fold. A meticulous inspection of the growth and changed data of individual OFGs is presented in Table S1.

Numerous fractures, microcracks, and cleavages are produced, effectively transforming the coal body from a closed system to an open system during the formation of TDC.[48] This structural transformation forms fragmented and finely powdered coal particles, accompanied by a marked increase in the internal surface area of primary pores, particularly micropores. The surfaces of TDC-8 and its TDC-based AC series exhibit enhanced reagent accessibility, promoting extensive reactions and the incorporation of additional OFGs during activation and subsequent acid modification.

Moreover, the total number of OFGs introduced in HNO_3-modified CACs is higher than those introduced in H_2SO_4−APS-modified CACs. Figure 5b indicates that HNO_3 treatment substantially augments carboxyl groups, followed by lactones and phenolic functional groups. By contrast, H_2SO_4−APS treatment introduces more lactones than carboxylic and phenolic groups in the order of lactones > carboxylic groups > phenolic groups.

3.2.3. XPS Characteristics of Coal and CAC Samples. Figure 6a displays the XPS spectra of the coal and six CAC samples. C 1s and O 1s are the two main peaks with remarkable heights. Figure 6b−g shows the deconvolution of the O 1s region of the CAC series, aiding in the identification of the changes in surface OFGs before and after modification.[75] Table S2 presents the XPS results. The degree of surface oxidation was determined by calculating the ratio of total oxygen to total carbon (O_{total}/C_{total}).

Figure 6a indicates that the main peaks of CACs are higher than those of the coals. The orders of O 1s peak heights are PSC-8 < PSC-8A < PSC-8AS < PSC-8AN and TDC-8 < TDC-8A < TDC-8AS < TDC-8AN. The O 1s peak height of TDC-8 is lower than that of PSC-8, while the TDC-based AC series has higher values than those of PSC-based AC series. TDC becomes soft and changes its chemical structure owing to the geological tectonic action. The surface OFG content decreases and is lower than that of the symbiotic PSC. The conversion of CAC inherits the softness of the coal body and the characteristics of nanoscale pores and SSAs, resulting in the introduction of excess OFGs. The oxygen content increases further after modification. The O 1s peak heights of PSC-8AS and TDC-8AS increase, while the C 1s peak decreases.

The O 1s spectra decompose into three peaks:[76,77] carbonyl C═O (531.0−531.9 eV; Peak 1), C−O hydroxyl groups, and noncarbonyl ether-type oxygen atoms in esters and anhydrides (532.3−532.8 eV; Peak 2), and carboxyl COO− (534.0−535.4 eV; Peak 3) peaks. Table S2 shows that PSC-8A and TDC-8A are dominated by Peak 3 with relative contents of 52.60 and 49.36%, followed by Peak 2 at 39.78 and 40.52%, respectively. The COO− content of both PSC-8AN and TDC-8AN increases to over 60%, and notably, TDC-8AN exhibits a higher COO− content compared to PSC-8AN. However, the C−O and C═O contents of PSC-8AN and TDC-8AN decrease. The COO− content of PSC-8AS and TDC-8AS decreases to <38%, while the relative contents of C−O and C═O are increased, with the relative content of C−O increasing to 47.43 and 43.51%, respectively.

The O_{total}/C_{total} ratio represents the oxidation degree, indicating the relative oxygen content. Table S2 shows that PSC-8AN and PSC-8AS exhibit 53.26 and 39.84% higher O_{total}/C_{total} ratios, respectively, than PSC-8A. Similarly, TDC-8AN and TDC-8AS show 66.19 and 45.87% higher O_{total}/C_{total} ratios, respectively, than TDC-8A. The orders of O_{total}/C_{total} of CACs are PSC-8A < PSC-8AS < PSC-8AN and TDC-8A < TDC-8AS < TDC-8AN, consistent with the O 1s peak height and Boehm titration results. The TDC-based AC series are more active than the PSC-based AC series in terms of the fluctuation range of three functional group contents, irrespective of whether the amount is increased or decreased.

3.3. Methane Adsorption Properties and Analysis of Coal and CAC Samples. PSC-8 is dominated by transitional pores, while TDC-8 has micropores (5−15 nm), mild micropores (2.5−5 nm), and ultramicropores (<2.5 nm), which determine methane adsorption capacity.[27,61] Ultramicropores dominate the SSA of TDC-8. The phased increase in the SSA of coal (Table 3) indicates that the gas adsorption capacity of TDC increases owing to the rapid increase in the ultramicroporous surface area. The amount of mesopores (2−50 nm) and micropores (<2 nm) of CAC significantly increases after transformation. Although the classification criteria of nanopores in coal and CAC might vary, a remarkable similarity exists in the pore size of the ultramicropores of coal

https://doi.org/10.1021/acsomega.4c00978
ACS Omega 2024, 9, 33510−33521

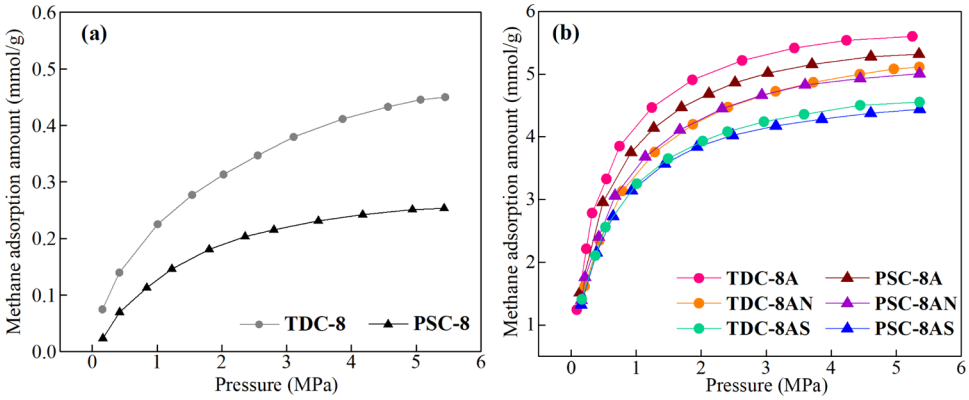

Figure 7. Adsorption isotherms of coal samples (a) and the CAC series (b).

and the micropores of CAC. In addition, a few macromolecules exist on the surface of CAC, and the influence of the molecules can be ignored for methane adsorption. Thus, the TDC homologous CAC serves as an effective amplification model for identifying and analyzing the changes in methane adsorption characteristics in TDCs.

The methane adsorption results (Table S3) were used to generate the isothermal adsorption curves of coal and CAC samples (Figure 7). The characteristics of the adsorption curves are consistent. The amount of adsorption in the low-pressure section increases rapidly with the equilibrium pressure, and then, the growth rate gradually reduces. The curve gradually flattens until it reaches its maximum value. Figure 7a shows that the methane adsorption of TDC-8 is approximately twice that of PSC-8 at the same temperature and pressure, indicating that TDC has a higher methane adsorption capacity than PSCs. Figure 7b demonstrates that the adsorption capacity of CAC for methane is 8−13-fold higher than those of the corresponding raw coal samples.

Figure 7b compares the methane adsorption curves of the CAC samples. Methane adsorption by TDC-8A is higher than that by PSC-8A, indicating that TDC-8A inherits strong methane adsorption capability. As previously discussed, HNO_3 increases the SSA and pore volume of CAC, whereas H_2SO_4−APS collapses and blocks the pores. Despite these contrasting effects, all modified CAC samples exhibit a marked decrease in methane adsorption, particularly the H_2SO_4−APS-treated CAC samples. Consistent results from FTIR, Boehm titration, and XPS analyses demonstrate that acidification enhances OFGs on the surface of CACs, which is in contrast to the expectation that the introduction of functional groups augments methane adsorption, suggesting that factors beyond changes in porosity might affect the adsorption process.

Acidic OFGs such as carboxyl, lactone, lactol, phenols, hydroxyl, and anhydride groups make the carbon surface hydrophilic,[43] which is unfavorable for the adsorption of methane, a nonpolar hydrophobic gas.[44] Our findings are in agreement with previous reports,[78,79] which confirm the inhibitory effect of acidic OFGs on methane adsorption. (i) The most active adsorption sites for methane reside on the surface of nanopores and at the juncture between nanopores. The augmented number of nanopores and the SSA furnish additional adsorption space for methane, forming the foundation and governing the methane adsorption capacity. (ii) Acidification increases the number of OFGs, increasing the negative charge and hydrophilicity on the pore surface,[43] which prevents hydrophobic methane adsorption.[44] (iii) The robust oxidation of modifiers induces the corrosion of pore walls, causing collapse and blockage, which is a secondary factor for decreasing methane adsorption capacity. The quantum chemical assessment of the negative charge on coal surfaces[80−82] speculates that carboxyl groups strongly inhibit methane adsorption, whereas lactones and phenolic groups weakly inhibit methane adsorption. In addition, the isotherm adsorption curves between TDC-8AN and PSC-8AN, as well as between TDC-8AS and PSC-8AS, display minimal disparities, with TDC-8AS even slightly lower than PSC-8AS. This implies that the identical acidification process nullifies the difference in methane adsorption capacity between PSC- and TDC-based CACs.

A few reports indicated an increased methane adsorption by acid-modified samples. For example, Song et al.[83] modified commercial CAC using acetic acid, which increased the surface area, total pore volume, and micropore volume, and decreased the micropore diameter. The increased CO_2 and CH_4 adsorption was attributed to either increased porosity or introduction of OFGs, which remains ambiguous. Notably, acetic acid is a weaker acid than the HNO_3 and H_2SO_4 used in our study. Strong acids are expected to introduce OFGs rapidly, which strongly inhibits methane adsorption. Thus, the suppression of methane adsorption by OFGs might outweigh the enhancing effect of increased microporosity in the case of strong acid modification, as in our study. This underscores the need for further investigation into the mechanistic aspects of acid-induced changes in methane adsorption, providing a promising avenue for future research.

4. CONCLUSIONS

Homologous CAC samples were used as a simplified enlarged model for coal with complex structures, especially tectonic coal, and were subjected to HNO_3 and H_2SO_4−APS modifications for studying the impact on methane adsorption characteristics. The results are as mentioned.

(i) Tectonic deformation converted porous coal into micropores, mild micropores, and ultramicropores with ultramicropores responsible for methane adsorption. The micropore volume and SSA of CACs increased sharply. The various pore parameters of the TDC-based AC series were higher than those of the corresponding PSC-based AC series.

(ii) A less concentrated HNO_3 expanded the pores, while the strong oxidizing properties of H_2SO_4−APS corroded the pore walls, finally collapsing and clogging some

https://doi.org/10.1021/acsomega.4c00978
ACS Omega 2024, 9, 33510−33521

nanopores. OFGs introduced by HNO_3 (carboxyl > lactone > phenol groups) were higher than those introduced by H_2SO_4–APS (lactone > carboxyl > phenol groups). The increase in OFGs on the surface of DC-based AC series is higher than that on PSC-based AC series.

(iii) The impact of micropore development and the SSA on methane adsorption is fundamental in determining the capacity for methane adsorption. The impact of reduced methane adsorption by increased OFGs is considerably higher than the enhanced methane adsorption by the increased micropore volume and SSA. OFGs are the primary cause for the decrease in methane adsorption capacity, while pore wall corrosion plays a secondary role.

(iv) This study highlights the unique advantages and tremendous potential of TDCs in producing ACs, offering new insights into the high value-added utilization of China's abundant tectonic coal resources and the development of high-performance coal-based methane storage materials.

■ ASSOCIATED CONTENT

Supporting Information

The Supporting Information is available free of charge at https://pubs.acs.org/doi/10.1021/acsomega.4c00978.

Detailed test data from Figures 5–7 are provided to aid in a comprehensive understanding and validation of the experimental results (PDF)

■ AUTHOR INFORMATION

Corresponding Author

Xiaojie Guo − *North China Institute of Science and Technology, Sanhe, Hebei 065201, P. R. China;* orcid.org/0000-0001-9373-5417; Email: guoxiaojiee@163.com

Authors

Xuan Huan − *Institute of Disaster Prevention Science and Safety Technology, Sanhe, Hebei 065201, P. R. China;* orcid.org/0000-0002-1938-0408

Xuexi Chen − *North China Institute of Science and Technology, Sanhe, Hebei 065201, P. R. China*

Xin Guo − *Chinese Institute of Coal Science, Hepingli, Beijing 100013, P. R. China*

Complete contact information is available at: https://pubs.acs.org/10.1021/acsomega.4c00978

Notes

The authors declare no competing financial interest.

■ ACKNOWLEDGMENTS

The author(s) disclosed receipt of the following financial support for the research, authorship, and/or publication of this article: This work was supported by the National Natural Science Foundation of China (nos. 52174181, 42102226, 52074121), the Fundamental Research Funds for the Central Universities (nos. 3142023014 and ZY20220210), the Langfang Science and Technology Research and Development Program (no. 2022013090), and the Science and Technology Project of Hebei Education Department (grant number ZC2023054). Sincere thanks go to the National Institute of Clean and Low Carbon Energy for their experimental support. The views and opinions expressed in this paper are those of the authors.

■ REFERENCES

(1) Chattaraj, S.; Mohanty, D.; Kumar, T.; Halder, G. Thermodynamics, kinetics and modeling of sorption behaviour of coalbed methane−A review. *J. Unconv. Oil Gas Resour.* **2016**, *16*, 14−33.

(2) Fan, C. J.; Li, S.; Luo, M. K.; Du, W. Z.; Yang, Z. H. Coal and gas outburst dynamic system. *Int. J. Min. Sci. Technol.* **2017**, *27* (1), 49−55.

(3) Cheng, Y. P.; Pan, Z. J. Reservoir properties of Chinese tectonic coal: A review. *Fuel* **2020**, *260*, No. 116350.

(4) Zhang, J. F.; Lin, H. F.; Li, S. G.; Yang, E. H.; Ding, Y.; Bai, Y.; Zhou, Y. X. Accurate gas extraction (AGE) under the dual-carbon background: Green low-carbon development pathway and prospect. *J. Cleaner Prod.* **2022**, *377*, No. 134372.

(5) Xu, F. Y.; Hou, W.; Xiong, X. Y.; Xu, B. R.; Wu, P.; Wang, H. Y.; Feng, K.; Yun, J.; Li, S. G.; Zhang, L.; Yan, X.; Fang, H. J.; Lu, Q.; Mao, D. L. The status and development strategy of coalbed methane industry in China. *Pet. Explor. Dev.* **2023**, *50* (4), 765−783.

(6) Zhang, B.; Liu, P.; Huang, Z. R.; Liu, J. J. Adsorption equilibrium and diffusion of CH_4, CO_2, and N_2 in coal-based activated carbon. *ACS Omega* **2023**, *8* (11), 10303−10313.

(7) Qin, Y.; Shen, J.; Shi, R. Strategic value and choice on construction of large CMG industry in China. *J. China Coal Soc.* **2022**, *47* (1), 371−387.

(8) Liu, D. M.; Qiu, F.; Liu, N.; Cai, Y. D.; Guo, Y. L.; Zhao, B.; Qiu, Y. K. Pore structure characterization and its significance for gas adsorption in coals: A comprehensive review. *Unconv. Resour.* **2022**, *2*, 139−157.

(9) Wang, C. H.; Cheng, Y. P. Role of coal deformation energy in coal and gas outburst: A review. *Fuel* **2023**, *332* (1), No. 126019, DOI: 10.1016/j.fuel.2022.126019.

(10) Rodrigues, C. F.; Lemos de Sousa, M. J. The measurement of coal porosity with different gases. *Int. J. Coal Geol.* **2002**, *48* (3−4), 245−251.

(11) Qiu, F.; Liu, D. M.; Cai, Y. D.; Liu, N.; Qiu, Y. K. Methane adsorption interpreting with adsorption potential and its controlling factors in various rank coals. *Processes* **2020**, *8* (4), 390.

(12) Wei, Q.; Li, X. Q.; Zhang, J. Z.; Hu, B. L.; Zhu, W. W.; Lian, W. L.; Sun, K. X. Full-size pore structure characterization of deep-buried coals and its impact on methane adsorption capacity: a case study of the Shihezi Formation coals from the Panji Deep Area in Huainan Coalfield, Southern North China. *J. Pet. Sci. Eng.* **2019**, *173*, 975−989.

(13) Song, W. H.; Yao, J.; Ma, J. S.; Li, A. F.; Li, Y.; Sun, H.; Zhang, L. Grand canonical Monte Carlo simulations of pore structure influence on methane adsorption in micro-porous carbons with applications to coal and shale systems. *Fuel* **2018**, *215* (6), 196−203.

(14) Li, Z. B.; Ren, T.; Li, X. C.; Qiao, M.; Yang, X. H.; Tan, L. H.; Nie, B. S. Multi-scale pore fractal characteristics of differently ranked coal and its impact on gas adsorption. *Int. J. Min. Sci. Technol.* **2023**, *33* (4), 389−401.

(15) Jia, G.; Yang, M.; Zhang, X. B.; Liu, L. Experimental Study on the pore structure of middle-and low-rank coal and its influence on methane adsorption. *Geofluids* **2022**, *2022*, No. 1372243, DOI: 10.1155/2022/1372243.

(16) Yang, H.; Bi, W. Y.; Zhang, Y. G.; Yu, J. K.; Yan, J. W.; Lei, D. J.; Ma, Z. N. Effect of tectonic coal structure on methane adsorption. *J. Environ. Chem. Eng.* **2021**, *9*, No. 106294.

(17) Zhang, J. J.; Wei, C. T.; Zhao, C. J.; Zhang, T.; Lu, G. W.; Zou, M. J. Effects of nano−pore and macromolecule structure of coal samples on energy parameters variation during methane adsorption under different temperature and pressure. *Fuel* **2021**, *289*, No. 119804.

(18) Sun, Y. F.; Zhao, Y. X.; Yuan, L. Impact of coal composition and pore structure on gas adsorption: a study based on a synchrotron radiation facility. *Greenhouse Gases* **2020**, *10* (1), 116−129.

(19) Liu, X. W.; Gu, Y. M.; Sun, T. J.; Guo, Y.; Wei, X. L.; Zhao, S. S.; Wang, S. D. Water resistant and flexible MOF materials for highly efficient separation of methane from nitrogen. *Ind. Eng. Chem. Res.* **2019**, *58* (44), 20392−20400.
(20) Li, T.; Luo, S. Z.; Wu, Y. Y.; Ni, H. Z. Study of the modifying of activated carbon and its adsorption properties of CO_2/CH_4 mixture. *J. China Coal Soc.* **2011**, *36* (12), 2012−2017.
(21) Cao, D. Y.; Li, X. M.; Zhang, S. R. Influence of tectonic stress on coalification: Stress degradation mechanism and stress polycondensation mechanism. *Sci. China, Ser. D: Earth Sci.* **2007**, *50* (1), 43−54.
(22) Pan, J. N.; Wang, S.; Ju, Y. W.; Hou, Q. L.; Niu, Q. H.; Wang, K.; Li, M.; Shi, X. H. Quantitative study of the macromolecular structures of tectonically deformed coal using high−resolution transmission electron microscopy. *J. Nat. Gas Sci. Eng.* **2015**, *27* (3), 1852−1862.
(23) Shepherd, J.; Rixon, L. K.; Griffiths, L. Outbursts and geological structure in coal mines: A review. *Int. J. Rock Mech. Min. Sci. Geomech. Abstr.* **1981**, *18* (4), 267−283.
(24) Cao, Y. X.; Davis, A.; Liu, R. X.; Liu, X. W.; Zhang, Y. G. The influence of tectonic deformation on some geochemical properties of coals−a possible indicator of outburst potential. *Int. J. Coal Geol.* **2003**, *53* (2), 69−79.
(25) Liu, D. M.; Yao, Y. B.; Tang, D. Z.; Tang, S. H.; Che, Y.; Huang, W. H. Coal reservoir characteristics and coalbed methane resource assessment in Huainan and Huaibei coalfields, Southern North China. *Int. J. Coal Geol.* **2009**, *79* (3), 97−112.
(26) Jiangwei, Y.; Wang, W.; Tan, Z. H. Distribution characteristics of gas outburst coal body in Pingdingshan tenth coal mine. *Procedia Eng.* **2012**, *45* (1), 329−333.
(27) Ju, Y. W.; Jiang, B.; Hou, Q. L.; Tan, Y. J.; Wang, G. L.; Xiao, W. J. Behavior and mechanism of the adsorption/desorption of tectonically deformed coals. *Chin. Sci. Bull.* **2009**, *54* (1), 88−94.
(28) Ju, Y. W.; Sun, Y.; Tan, J. Q.; Bu, H. L.; Han, K.; Li, X. S.; Fang, L. Z. The composition, pore structure characterization and deformation mechanism of coal-bearing shales from tectonically altered coalfields in eastern China. *Fuel* **2018**, *234*, 626−642.
(29) Song, Y.; Jiang, B.; Li, M.; Hou, C. L.; Xu, S. C. A review on pore-fractures in tectonically deformed coals. *Fuel* **2020**, *278*, No. 118248.
(30) Hou, Q. L.; Li, H. J.; Fan, J. J.; Ju, Y. W.; Wang, T. K.; Li, X. S.; Wu, Y. D. Structure and coalbed methane occurrence in tectonically deformed coals. *Sci. China Earth Sci.* **2012**, *55* (11), 1755−1763.
(31) Zhou, H. X.; Yang, Q. L.; Cheng, Y. P.; Ge, C. G.; Chen, J. X. Methane drainage and utilization in coal mines with strong coal and gas outburst dangers: A case study in Luling mine, China. *J. Nat. Gas Sci. Eng.* **2014**, *20*, 357−365.
(32) Lan, J. M.; Wang, B. Y.; Bo, C. M.; Gong, B. L.; Ou, J. J. Progress on fabrication and application of activated carbon sphere in recent decade. *J. Ind. Eng. Chem.* **2023**, *120*, 47−72.
(33) Zheng, Y. N.; Li, S. S.; Jiang, B. Y.; Yu, G. F.; Ren, B.; Zheng, H. T. One-step preparation of activated carbon for coal bed methane separation/storage and its methane adsorption characteristics. *ACS Omega* **2022**, *7* (49), 45107−45119.
(34) Sultana, M.; Rownok, M. H.; Sabrin, M.; Rahaman, M. H.; Alam, S. M. N. A review on experimental chemically modified activated carbon to enhance dye and heavy metals adsorption. *Cleaner Eng. Technol.* **2022**, *6*, No. 100382.
(35) Feng, Y. Y.; Huang, L. H.; Chu, W. Surface modification of coal based activated carbon and its effects on methane adsorption. *J. China Coal Soc.* **2012**, *36* (12), 2080−2085.
(36) Guo, X. J.; Huan, X.; Huan, H. H. Structural characteristics of deformed coals with different deformation degrees and their effects on gas adsorption. *Energy Fuels* **2017**, *31*, 13374−13381.
(37) Guo, D. Y.; Guo, X. J. The influence factors for gas adsorption with different ranks of coals. *Adsorpt. Sci. Technol.* **2018**, *36* (3−4), 904−918.
(38) Huan, X.; Zhang, X. B.; Wei, H. W. Research on parameters of adsorption potential via methane adsorption of different types of coal. *J. China Coal Soc.* **2015**, *40* (8), 1859−1864.
(39) Zhang, X. B.; Wang, W.; Zhang, Y. G.; Huan, X. Oriented growth mechanism of tectonic coal microcrystal. *J. China Coal Soc.* **2016**, *41* (3), 712−718.
(40) Li, H. Y. Major and minor structural features of a bedding shear zone along a coal seam and related gas outburst, Pingdingshan coalfield, northern China. *Int. J. Coal Geol.* **2001**, *47* (2), 101−113.
(41) Okolo, G. N.; Neomagus, H. W. J. P.; Everson, R. C.; Roberts, M. J.; Bunt, J. R.; Sakurovs, R.; Mathews, J. P. Chemical−structural properties of South African bituminous coals: insights from wide angle XRD−carbon fraction analysis, ATR−FTIR, solid state ^{13}C NMR, and HRTEM techniques. *Fuel* **2015**, *158*, 779−792.
(42) Singh, G.; Ruban, A. M.; Geng, X.; Vinu, A. Recognizing the potential of K−salts, apart from KOH, for generating porous carbons using chemical activation. *Chem. Eng. J.* **2023**, *451*, No. 139045.
(43) Alcañiz-Monge, J.; Román-Martínez, M. D. C.; Lillo-Ródenas, M. Á. Chemical Activation of Lignocellulosic Precursors and Residues: What Else to Consider? *Molecules* **2022**, *27* (5), 1630−1656.
(44) Wang, X. H.; Cheng, H. R.; Ye, G. Z.; Fan, J.; Yao, F.; Wang, Y. Q.; Jiao, Y. J.; Zhu, W. F.; Huang, H. M.; Ye, D. Q. Key factors and primary modification methods of activated carbon and their application in adsorption of carbon−based gases: A review. *Chemosphere* **2022**, *287* (2), No. 131995.
(45) Polovina, M.; Babić, B.; Kaluderović, B.; Dekanski, A. Surface characterization of oxidized activated carbon cloth. *Carbon* **1997**, *35* (8), 1047−1052.
(46) Gil, A.; Puente, G. D. L.; Grange, P. Evidence of textural modifications of an activated carbon on liquid-phase oxidation treatments. *Microporous Mater.* **1997**, *12* (1−3), 51−61.
(47) Kruk, M.; Jaroniec, M.; Gilpin, R. K.; Zhou, Y. W. Nitrogen adsorption studies of coated and chemically modified chromatographic silica gels. *Langmuir* **1997**, *13* (3), 545−550.
(48) Ren, J. G.; Song, Z. M.; Li, B.; Liu, J. B.; Lv, R. S.; Liu, G. F. Structure feature and evolution mechanism of pores in different metamorphism and deformation coals. *Fuel* **2021**, *283*, No. 119292.
(49) Brunauer, S.; Emmett, P. H.; Teller, E. Adsorption of gases in multimolecular layers. *J. Am. Chem. Soc.* **1938**, *60* (2), 309−319.
(50) Gregg, S. J.; Sing, K. S. W.; Salzberg, H. W. Adsorption surface area and porosity. *J. Electrochem. Soc.* **1967**, *114* (11), No. 279CA, DOI: 10.1149/1.2426447.
(51) Kakei, K.; Ozeki, S.; Suzuki, T.; Kaneko, K. Multi-stage micropore filling mechanism of nitrogen on microporous and micrographitic carbons. *J. Chem. Soc., Faraday Trans.* **1990**, *86*, 371−376.
(52) He, X. Q.; Liu, X. F.; Song, D. Z.; Nie, B. S. Effect of microstructure on electrical property of coal surface. *Appl. Surf. Sci.* **2019**, *483*, 713−720.
(53) Song, D. Z.; Liu, X. F.; He, X. Q.; Nie, B. S.; Wang, W. Investigation on the surface electrical characteristics of coal and influencing factors. *Fuel* **2021**, *287*, No. 119551.
(54) Boehm, H. P. Chemical identification of surface groups. *Adv. Catal.* **1966**, *16*, 179−274.
(55) Zhao, G. F.; Bai, P.; Zhu, H. Y.; Yan, R.; Liu, X. M.; Yan, Z. F. The modification of activated carbons and the pore structure effect on enrichment of coal-bed methane. *Asia-Pac. J. Chem. Eng.* **2008**, *3* (3), 284−291.
(56) Jaramillo, J.; Alvarez, P. M.; Gomez-Serrano, V. Oxidation of activated carbon by dry and wet methods: Surface chemistry and textural modifications. *Fuel Process. Technol.* **2010**, *91* (11), 1768−1775.
(57) Shafeeyan, M. S.; Daud, W. M. A. W.; Houshmand, A.; Shamiri, A. A review on surface modification of activated carbon for carbon dioxide adsorption. *J. Anal. Appl. Pyrolysis* **2010**, *89* (2), 143−151.
(58) Sing, K. S. W.; Everett, D. H.; Haul, R. A. W.; Moscou, L.; Pierotti, R. A.; Rouquérol, J.; Siemieniewska, T. Reporting physisorption data for gas/solid systems with special reference to

the determination of surface area and porosity. *Pure Appl. Chem.* **1985**, *57* (4), 603−619.
(59) Ju, Y. W.; Jiang, B.; Hou, Q. L.; Wang, L. G.; Fang, A. M. Structural evolution of nano−scale pores of tectonic coals in Southern North China and its mechanism. *Acta Geol. Sin* **2005**, *79*, 269−285.
(60) Yu, S.; Jiang, B.; Li, F. L.; Liu, J. G. Structure and fractal characteristic of micro−and mesopores in low, middle−rank tectonic deformed coals by CO_2 and N_2 adsorption. *Microporous Mesoporous Mater.* **2017**, *253*, 191−202.
(61) Yu, S.; Jiang, B.; Liu, J. G. Nanopore structural characteristics and their impact on methane adsorption and diffusion in low to medium tectonically deformed coals: case study in the Huaibei coal field. *Energy Fuels* **2017**, *31* (7), 6711−6723.
(62) Qi, L. L.; Tang, X.; Wang, Z. F.; Peng, X. S. Pore characterization of different types of coal from coal and gas outburst disaster sites using low temperature nitrogen adsorption approach. *Int. J. Min. Sci. Technol.* **2017**, *27* (2), 371−377.
(63) Gaylord, N. G.; Eirich, F. R. The structure and properties of porous materials. *J. Polym. Sci.* **1960**, *45* (145), 278−279.
(64) Li, M.; Jiang, B.; Lin, S. F.; W, J. L.; Ji, M. J.; Qu, Z. H. Tectonically deformed coal types and pore structures in Puhe and Shanchahe coal mines in western Guizhou. *Min. Sci. Technol.* **2011**, *21* (3), 353−357.
(65) Lu, G. W.; Wei, C. T.; Wang, J. L.; Meng, R. Y.; Tamehe, L. S. Influence of pore structure and surface free energy on the contents of adsorbed and free methane in tectonically deformed coal. *Fuel* **2021**, *285*, No. 119087.
(66) Hamyali, H.; Nosratinia, F.; Rashidi, A.; Ardjmand, M. Anthracite coal−derived activated carbon as an effectiveness adsorbent for superior gas adsorption and CO_2/N_2 and CO_2/CH_4 selectivity: Experimental and DFT study. *J. Environ. Chem. Eng.* **2022**, *10* (1), No. 107007.
(67) Painter, P. C.; Snyder, R. W.; Starsinic, M.; Coleman, M. M.; Kuehn, D. W.; Davis, A. Concerning the application of FTIR to the study of coal: a critical assessment of band assignment and the application of spectral analysis programs. *Appl. Spectrosc.* **1981**, *35*, 475−485.
(68) Geng, W. H.; Nakajima, T.; Takanashi, H.; Ohki, A. Analysis of carboxyl group in coal and coal aromaticity by fourier transform infrared (FT−IR) spectrometry. *Fuel* **2009**, *88* (1), 139−144.
(69) Song, Y.; Jiang, B.; Han, Y. Z. Macromolecular response to tectonic deformation in low−rank tectonically deformed coals (TDCs). *Fuel* **2018**, *219*, 279−287.
(70) Painter, P. C.; Sobkowiak, M.; Youtcheff, J. FT−IR study of hydrogen bonding in coal. *Fuel* **1987**, *66* (7), 973−978.
(71) Chen, J. P.; Wu, S. N. Acid Base−treated activated carbons: characterization of functional groups and metal adsorptive properties. *Langmuir* **2004**, *20* (6), 2233−2224.
(72) Machnikowska, H.; Krzton, A.; Machnikowski, J. The characterization of coal macerals by diffuse reflectance infrared spectroscopy. *Fuel* **2002**, *81* (2), 245−252.
(73) Fanning, P. E.; Vannice, M. A. A drifts study of the formation of surface groups on carbon by oxidation. *Carbon* **1993**, *31* (5), 721−730.
(74) Wang, Z.-M.; Yamashita, N.; Wang, Z. X.; Hoshinoo, K.; Kanoh, H. Air oxidation effects on mlcroporosity, surface property, and CH_4 adsorptivity of pltch−basedactlvated carbon fibers. *J. Colloid Interface Sci.* **2004**, *276* (1), 143−150.
(75) Cuervo, M. R.; Asedegbega-Nieto, E.; Díaz, E.; Ordóñez, S.; Vega, A.; Dongil, A. B.; Rodríguez-Ramos, I. Modification of the adsorption properties of high surface area graphites by oxygen functional groups. *Carbon* **2008**, *46* (15), 2096−2106.
(76) Figueiredo, J. L.; Pereira, M. F. R.; Freitas, M. M. A.; Órfão, J. J. M. Modification of the surface chemistry of activated carbons. *Carbon* **1999**, *37* (9), 1379−1389.
(77) Zhou, J. H.; Sui, Z. J.; Zhu, J.; Li, P.; Chen, D.; Dai, Y. C.; Yuan, W. K. Characterization of surface oxygen complexes on carbon nanofibers by TPD, XPS and FT−IR. *Carbon* **2007**, *45* (4), 785−796.
(78) Feng, Y. Y.; Yang, W.; Liu, D. J.; Chu, W. Surface modification of bituminous coal and its effects on methane adsorption. *Chin. J. Chem.* **2013**, *31* (8), 1102−1108.
(79) Hao, S. X.; Wen, J.; Yu, X. P.; Chu, W. Effect of the surface oxygen groups on methane adsorption on coals. *Appl. Surf. Sci.* **2013**, *264*, 433−442.
(80) Wang, B.; Li, M.; Zhao, Q. Y.; Qin, Y. H.; Xie, K. C. Relationship between surface potential and functional groups of coals. *J. Chem. Ind. Eng.* **2004**, *55* (8), 1329−1333.
(81) Crawford, R. J.; Mainwaring, D. E. The influence of surfactant adsorption on the surface characterisation of Australian coals. *Fuel* **2001**, *80* (3), 313−320.
(82) Li, H.; Wei, S. Q.; Qing, C. L.; Yang, J. S. Discussion on the position of the shear plane. *J. Colloid Interface Sci.* **2003**, *258* (1), 40−44.
(83) Song, X.; Wang, L. A.; Zeng, Y. M.; Zhan, X. Y.; Gong, J.; Li, T. Application of activated carbon modified by acetic acid in adsorption and separation of CO_2 and CH_4. *AIP Conf. Proc.* **2018**, *1944*, No. 020056.

https://doi.org/10.1021/acsomega.4c00978
ACS Omega 2024, 9, 33510−33521